JAHRBUCH DER GEOLOGISCHEN BUNDESANSTALT

Jb. Geol. B.-A. | ISSN 0016–7800 | Band **140** | Heft 1 | S. 29–45 | Wien, September 1997

Mudturbidites, Black Shales and Bentonites from the Paleocene/Eocene Boundary: the Anthering Formation of the Rhenodanubian Flysch (Austria)

HANS EGGER, MAX BICHLER, ILSE DRAXLER, MANDANA HOMAYOUN, HEINZ-JÜRGEN HUBER, ELISABETH Ch. KIRCHNER, PETER KLEIN, ROUBEN SURENIAN*)

6 Text-Figures, 5 Tables and 3 Plates

Salzburg
Rhenodanubischer Flysch
Anthering-Formation
Sedimentologie
Stratigraphie
Nannoplankton
Palynologie

Österreichische Karte 1 : 50.000
Blatt 63

Inhalt

Schlammturbidite, schwarze Tonschiefer und Bentonite von der Paleozän/Eozän-Grenze: Die Anthering-Formation im Rhenodanubischen Flysch (Österreich)

Zusammenfassung

An der Typlokalität der Anthering-Formation wurden folgende Nannoplankton-Zonen nachgewiesen: *Discoaster multiradiatus*-Zone, *Tribrachiatus contortus*-Zone und *Discoaster binodosus*-Zone. Diese entsprechen den Zonen NP9, NP10 und NP11 in der Gliederung von MARTINI (1971). Im Gegensatz zu der liegenden Altlengbach-Formation, die meist reichlich Hartbänke aufweist, ist die Anthering-Formation durch das Vorherrschen von karbonatreichen Schlammturbiditen (weiche siltführende Mergel) und darin gelegentlich eingeschaltete Schwarzschiefer (Tonsteine) charakterisiert. Dieser Wechsel in der Sedimentfazies (Abnahme des terrigenen Materials bei gleichzeitiger Zunahme des Karbonatgehaltes) wird als Folge einer Transgression am Ende des Paleozäns interpretiert. Die pelitischen Gesteine der Anthering-Formation weisen hohe Gehalte an Smektit auf und innerhalb der hemipelagischen Tonsteine treten mehr als zwanzig Lagen von reinem Montmorillonit auf. Diese bis 3 cm mächtigen Bentonite werden als Tuffe interpretiert, die aus Aschenregen hervorgegangen sind. Sie sind auf den ältesten Abschnitt der Zone NP10 beschränkt. Die Gehalte an immobilen Elementen (Ti, Zr, Nb, Y) der meisten Bentonitlagen verweisen auf alkalibasaltische Magmenzusammensetzungen, während einige der mächtigeren Lagen auf trachytische Eruptionen zurückgehen dürften. Das Alter der Aschenlagen und ihre chemische Zusammensetzung machen eine Korrelation mit Bentoniten aus Nordeuropa wahrscheinlich.

*) Authors' addresses: Dr. HANS EGGER, Dr. ILSE DRAXLER, Dr. MANDANA HOMAYOUN, Dr. PETER KLEIN, Dr. ROUBEN SURENIAN, Geologische Bundesanstalt, Rasumofskygasse 23, A-1031 Wien; Univ.-Doz. MAX BICHLER, HEINZ-JÜRGEN HUBER: Atominstitut der österreichischen Universitäten, Schüttelstraße 115, A-1020 Wien; Univ.-Prof. Dr. ELISABETH Ch. KIRCHNER: Institut für Mineralogie der Universität Salzburg, Hellbrunnerstraße 34, A-5020 Salzburg.

Abstract

At the type locality of the Anthering formation the following biozones have been recognized: *Discoaster multiradiatus* Zone, *Tribrachiatus contortus* Zone and *Discoaster binodosus* Zone. These biozones correspond to NP 9, NP 10 and NP 11 of the zonation of MARTINI (1971). Contrary to the underlying sand bearing Altlengbach formation the Anthering formation is characterized by the predominance of carbonate rich mudturbidites (silty marls) and occasionally intercalated black shales. This change in sedimentary facies (decrease of terrigeneous input, increase of carbonate contents) is seen as a consequence of a transgression at the end of the Paleocene. The pelitic rocks of the Anthering formation have high contents of smectite and even distinct bentonite layers were deposited together with the hemipelagites. These bentonites, which are interpreted as tuffs of air-fall derivation, are restricted to the lowermost part of NP 10. Chemical analyses suggest that the explosive magmas had an alkali basaltic composition. Single layers however show immobile element concentrations typical for highly evolved alkaline ashes. The age of the ash-bearing sequence and the chemical compositions of the bentonites point to a correlation with bentonites of the North Sea region.

1. Introduction

The Rhenodanubian Flyschzone constitutes a subunit of the Penninic nappe complex of the Eastern Alps. The Late Cretaceous to Early Eocene sediments of this flyschzone were deposited in a moderately converging remnant oceanic basin. Thin layers of green hemipelagic claystone between the sand- and silt-sized carbonate bearing turbidites reveal that this basin was located below the local calcite compensation depth (CCD).

In the area north and northeast of Salzburg the Anthering Formation (EGGER, 1995) forms the youngest part of the Rhenodanubian Flysch. The type locality of this formation is situated in the small gully of the Kohlbach 15 km north of Salzburg (Text-Fig. 1). A quarternary moraine covers the southern sector of the valley. The first outcrop of the Paleogene is located about 50 m upstream of the small roadbridge displaying sediments from the Early Eocene (NP 11). Unfortunately there is no continuously exposed section from here on upstream but there are a number of adjacent outcrops owing to

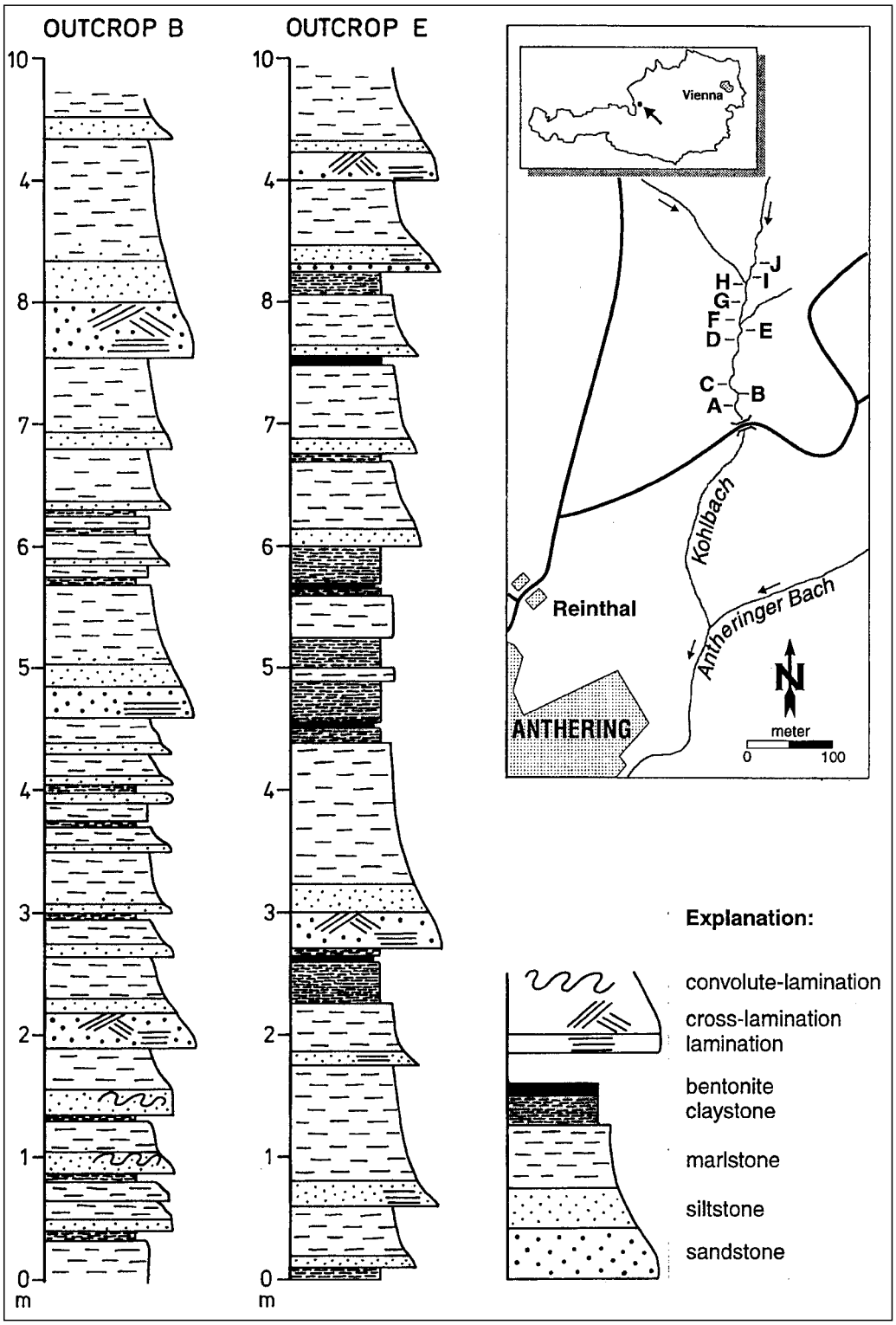

Text-Fig. 1.
Location of the outcrops and examples of the sedimentary facies of the Anthering formation.

the erosion at the outside bends of the meander loops. In all the exposures the beds are dipping steeply to south-southwest. To the north the Anthering formation is bordered by a tectonic fault. North of that fault the Late Paleocene (NP 9) of the Altlengbach formation is dipping north and is showing reverse bedding. Due to these tectonic complications the lower boundary of the Anthering formation is not exposed.

This paper summarizes the first results of biostratigraphic, geochemical and mineralogical investigations from the Anthering flysch section which is considered to be a stratigraphic section of the NP 9/NP 10 zonal boundary. This boundary is often used in marine sections as a proxy for the Paleocene/Eocene boundary and is dated with 55.0 Ma (SWISHER & KNOX, 1991). On the other hand planktonic foraminiferal specialists usually correlate the P5/P6 zonal boundary (AUBRY et al., 1996) which is estimated at 54.7 Ma with the Paleocene/Eocene boundary. More recently the major $\delta^{13}C$ spike at 55.5 Ma has been suggested as providing a useful means of correlation between marine and terrestric stratigraphies. In the deep sea this significant $\delta^{13}C$ excursion is associated with a world wide benthic foraminiferal extinction. Lacking a clearly defined Global Stratotype Section and Point (GSSP) the Paleocene/Eocene boundary still awaits a clear definition (see discussion in BERGGREN & AUBRY, 1996).

2. Lithostratigraphy of the Anthering Formation

2.1. Mudturbidites

In contrast to the underlying Altlengbach formation with its abundant sandstone and siltstone beds the Anthering formation is characterized by the predominance of soft graded silty marls and marls (Text-Fig. 1 and 2). They display average carbonate contents of approximately 40 % and average contents of organic carbon of 0.49 %. Occasionally these light grey coloured marls change into thin sandy layers towards their base. These usually display base-truncated BOUMA-sequences. Therefore the marly rocks can be interpreted as mud turbidites.

The single turbidite layers reach thicknesses up to 2 m. Sandy to silty hardbeds (calcareous greywackes) with complete BOUMA-sequences occur only sporadically within the section. They usually show well developed flute casts, which are indicating a sediment transport parallel to the basin axis from southwest to northeast. Therefore we can assume a deepening of the basin in that direction. Heavy mineral associations of these beds (det. W. SCHNABEL) are dominated by turmaline (31 %), apatite (25 %), zircone (17 %) and garnet (17 %). Very unusual for the Rhenodanubian flysch are high contents of apatite which indicate magmatic sources.

To study the clayminerals X-ray diffraction analyses were made from samples of the carbonate-free material after treatment with diluted acetic acid. A centrifuge was used for separating particle size fraction (<2 μm) and for the orientation of the platy minerals on glass slides. All samples were analyzed according to standard procedures (THOREZ, 1976; MOORE & REYNOLDS, 1989). The phases present in the different mudturbidite samples include smectite, illite, kaolinite and minor amounts of chlorite (Text-Fig. 3, Tab. 1). The most remarkable feature is the high content of authigenic smectite. The formation of this mineral can be explained by chemical weathering of volcanic components. Even pure montmorillonite layers (bentonites) occur in the section which are interpreted as ashes of air fall derivation (see chapter 2.3.). These layers are restricted to a short part of the section whereas smectite is common in the pelitic rocks of the entire section. The bentonites are seen as products of a short period of strongly increased explosive volcanic activity.

2.2. Hemipelagites

Usually the hemipelagic claystones of the Anthering formation are bioturbated, contain abundant agglutinated foraminifera and show green colour. Only within a short division of the Anthering section (outcrop E and a single layer in outcrop D – Text-Fig. 1) the light coloured turbidites contrast with alternating dark grey to black claystones. The single layers of these claystones can reach thicknesses up to 40 cm and are much thicker than other claystone layers of the section. Probably the reason for these remarkable thicknesses was the increased input of volcanic ash material. No fine scale lamination is visible in the claystones. From this homogenous fabric a continuous accumulation of the clay particles can be implied. The dark colour of the claystones is a result of relatively high contents of organic carbon (0.94 % on average) and of abundant pyrite. Under the electron microscope the studied samples of black shales from the Anthering section show abundant framboids and minute crystals of pyrite (s. Text-Fig. 4). Due to the weathering of sulphide the surfaces of the claystones show a rusty appearance and sometimes tiny gypsum crystals can be observed there. A strong sulphuric smell was noticed when grinding

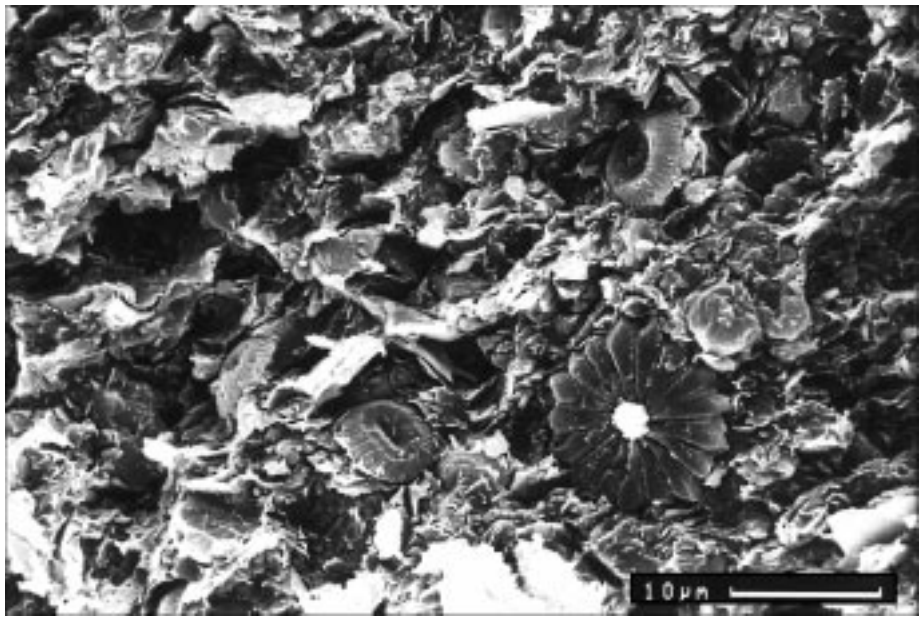

Text-Fig. 2.
Mudturbidite of the Anthering formation with abundant calcareous nannoplancton.

Table 1.
Mineralogical composition of turbidites (*) and hemipelagites from the Anthering formation.

Claymineralogy, siliciclastics, carbonates and sheetsilicates								
Sample	Smectite	Illite-mica	Kaolinite	Chlorite	Quartz	Feldspar	Carbonate	Sheetsilicates
1*	79%	15%	6%	0%	15%	0%	53%	32%
2	73%	21%	6%	0%	25%	2%	0%	73%
25*	48%	44%	5%	3%	20%	5%	13%	62%
27*	24%	36%	40%	0%	16%	2%	44%	38%
30*	71%	21%	8%	0%	15%	2%	47%	36%
80*	89%	7%	2%	2%	20%	0%	29%	51%
81*	90%	7%	3%	0%	7%	0%	44%	49%
82	98%	2%	0%	0%	10%	7%	0%	83%
83	93%	3%	2%	2%	17%	0%	0%	83%
84	81%	8%	11%	0%	15%	0%	0%	85%
85	78%	15%	5%	2%	23%	0%	0%	77%
89	81%	16%	0%	3%	17%	0%	2%	81%
12	25%	35%	40%	0%	40%	5%	4%	51%
13*	64%	30%	6%	0%	20%	2%	38%	40%
14	94%	2%	0%	4%	18%	3%	8%	71%
58	58%	36%	0%	6%	42%	14%	4%	40%
59	63%	10%	0%	27%	24%	5%	22%	49%
60	69%	14%	0%	17%	22%	4%	0%	74%
75*	79%	16%	3%	2%	18%	20%	43%	19%

the samples. Contrary to the turbiditic marls, which contain abundant foraminifera and calcareous nannoplankton, the claystone does not contain any planktonic organisms except pyritized remains of diatoms and radiolaria. There are also no hints of benthic foraminifera or of bioturbation. All these features led to an interpretation of these claystones as a hemipelagic sediment of an oxygen-deficient environment.

For reaching a better classification of the accumulation environment of the dark claystones some geochemical techniques were applied to get more paleoecological information. A variety of approaches has been proposed to recognize different degrees of bottom-water oxygenation. One of the most accepted methods is the determination of the degree of pyritization (DOP) which is the ratio of pyritic Fe to pyritic Fe plus acid-soluble Fe (RAISWELL et al., 1988). Under anoxic conditions seawater sulfate is reduced to H_2S, which reacts with detrital iron minerals and ultimately forms pyrite.

In ancient euxinic environments the extent of pyrite formation appears to be mainly limited by reactive iron content (DOP values generally exceed 0.75) while little pyrite

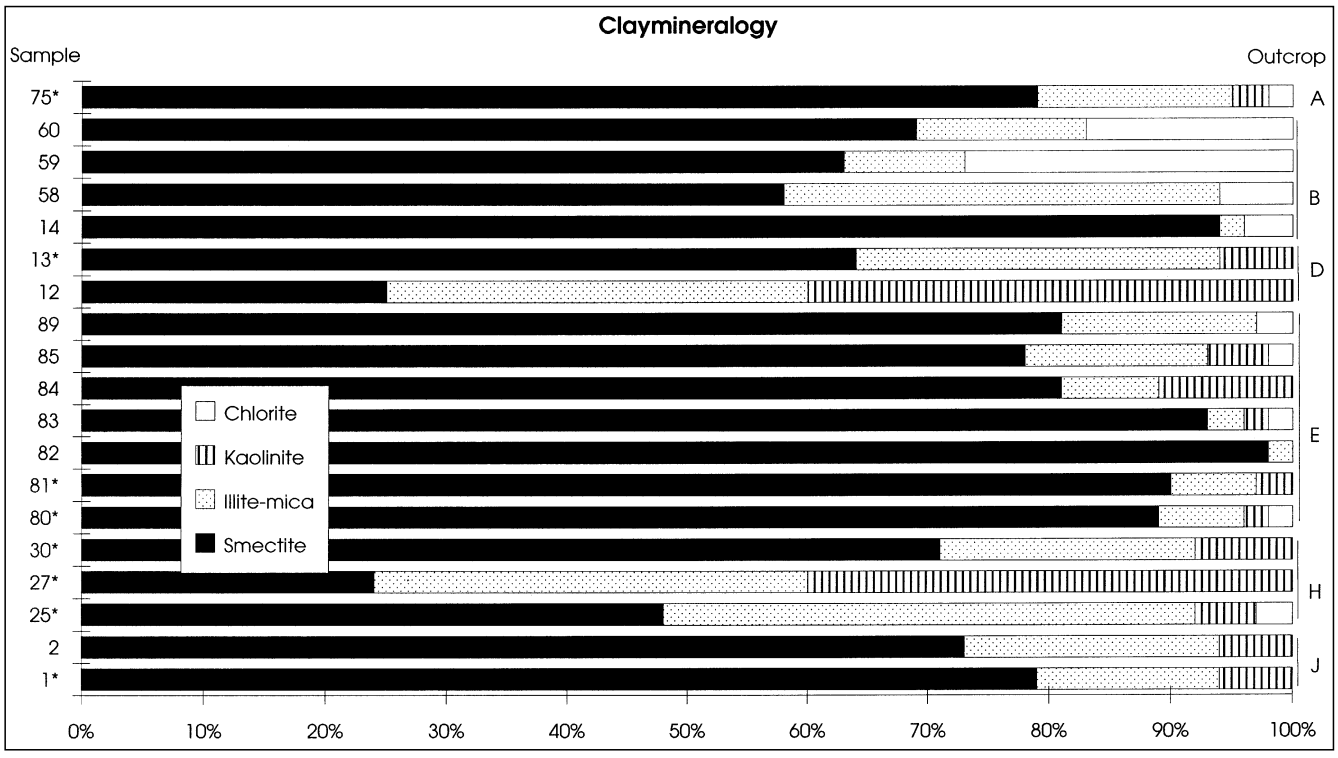

Text-Fig. 3.
Clay mineral composition of turbidites (*) and hemipelagites of the Anthering formation (see also Table 1).

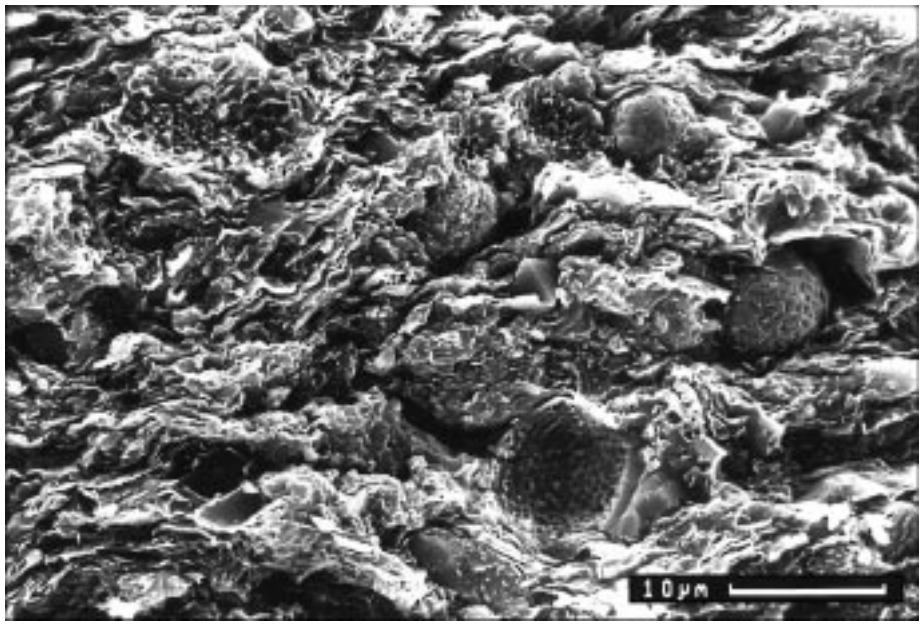

Text-Fig. 4.
SEM image of black shale from Anthering formation (outcrop E).
The homogenous fabric consists of parallel orientated platy particles of clay minerals with occasional pyrite framboids and pyrite octahedra.

is preserved in oxic settings where DOP values are consequently low (less than 0.5).

This hypothesis assumes that iron liberated in acid is potentially reactive toward sulfide. Therefore DOP values are usually determined by boiling the samples with concentrated HCl (see BERNER, 1970). Using this method, however, no reliable results were obtained for the samples from Anthering. So the highest DOP-values were found for the bentonite layers which actually do not contain any pyrite. Electrone microscope studies combined with energy dispersive X-ray analysis reveal that all the iron of the bentonites is bound in montmorillonite. Therefore the above mentioned technique for DOP determinations seems to be not valid for samples where iron is mainly bound in sheet silicates because this iron reacts too slowly with the hydrochloric-acid.

To get at least an approximate value for the DOP we assumed that all the sulfur is bound in pyrite and we used the sulfur values to calculate the contents of pyritic iron. The DOP values of the black shales of outcrop E indicate dysaerobic to anoxic paleoenvironmental conditions whereas the green shales of outcrop B were deposited under oxic conditions (Table 2). Occasionally within the same layer a change from black shale to weakly bioturbated green shale was observed. As the black shales mainly appear together with the bentonites these recurrent anoxia could be interpreted as the result of surface eutrophication by input of volcanic material.

As another indicator of paleoredox conditions the V/Cr index was introduced by DILL (1986). Vanadium is often enriched in black shales because the vanadyl cation is most stable under reducing acidic conditions. On the other hand Cr is entirely of detrital origin and it should not therefore fluctuate under redox conditions. For the black shales of outcrop E we calculated V/Cr values between 2.2 and 2.4. Values in excess of 2 should be diagnostic of anoxia.

Another trace metal which should be enriched in black shales is Uranium. Under anoxic depositional conditions uranium appears to precipitate as an authigenic element. According to the observation that in most marine shales deposited under oxic conditions $Th/U_{detrital}$ ratios range between 3 and 5 the authigenic U value (Ua) can be expressed as: $U_a = U_{total} - Th/3$ (WIGNALL, 1994). Using this calculation for the black shales from Anthering no proportion of authigenic U could be recognized. U values of the black shales are equivalent to those of green shales of outcrop B (see Table 1). Perhaps the absence of authigenic U is a consequence of the assumed low proportion of terrestric organic matter in this deep basin facies.

2.3. Bentonites

Around twenty white to yellowish bentonite layers were observed from the uppermost part of outcrop H to the uppermost part of outcrop E. As the section is not continuously exposed the total number of bentonites could be much higher. In a small exposure 800 m northwest of the described section we found 13 bentonite layers (y1–y13) which could not be correlated yet with the bentonites of the main section (×1–×22).

The bentonites can achieve thicknesses up to 3 cm but usually they are only a few millimeters thick. Therefore it was not possible to observe any sedimentary structures (e.g. graded bedding) within these layers in the field. Due to the fine-grained composition of the bentonites (Text-Fig. 5) it was not possible to analyze any isolated volcanic components or relicts.The layers consist essentially of Fe-montmorillonite and are interpreted as tuffs of air-fall derivation.

Owing to the thinness of the layers it is difficult to get enough uncontaminated material for chemical analyses. Three samples were analyzed for major elements, twenty-four samples were analyzed for trace elements (see Tables 3 and 4). Most Trace elements were determined by Neu-

	BLACK SHALES (outcrop E)			GREEN SHALES (outcrop B)		
	85	87	89	58	59	60
toc %	0,98	1,02	1,17	0,15	0,19	0,15
S %	2,52	3,28	2,28	0,1	0,12	0,03
Fe (tot) %	6,64	7,27	6,02	2,86	3,87	3,78
Fe (pyr) %	4,39	5,71	3,97	0,17	0,21	0,05
DOP	0,66	0,78	0,65	0,14	0,11	0,03
U ppm	3,1	2,9	2,6	1,6	2,4	2,8
V ppm	306	327	305	142	127	143

Table 2.
A comparison of some geochemical data of black shales and green shales.

Table 3.
Trace element concentrations of bentonite layers from the Anthering section.

ANTHERING BENTONITES															
x-values ppm, except declared with %															
	x1	x2	x4	x5	x6	x7	x8	x9	x10	x12	x13	x14	x15	x16	x17
Sc	8,00±0,40	31±1,5	17±0,85	27±1,35	22±1,1	15±0,75	28±1,4	25±1,25	21±1,05	42±2,1	39±1,9	19±0,99	26±1,3	33±1,6	29±1,5
Ti %	0,45±0,041	3,8±0,19								2,1±0,11	2,0±0,10	1,1±0,058	1,5±0,076	1,9±0,097	1,9±0,095
V	25±2,7	699±35	34±1,7	286±14,3	237±12	160±8	322±16,1	280±14	224±11	372±19	243±12	147±7,4	208±10	337±17	236±12
Cr	18±0,88	74±3,7	88±4,4	74±3,5	114±5,7	77±3,9	99±4,9	69±3,5	92±2,6	111±5,6	104±5,2	84±4,2	86±4,3	103±5,1	127±6,4
Mn	135±6,8	69±3,5								27±1,37	103±5,1	78±3,9	27±1,3	62±3,1	128±5,8
Co	3,5±0,17	11±0,59	21±1,05	26±1,3	28±1,4	13±0,65	23±1,15	43±2,15	12±0,6	23±1,2	22±1,1	75±3,7	29±1,4	55±2,8	6,4±0,3
Ni	62±8,1									65±7,8	61±7,3	169±8,5	64,19±6,4	103±5,2	38±1,9
Zn	74±3,7		120±6	42±2,1	148±7,4	103±5,1	234±11,7	323±16,15	149±7,3	163±8,1	152±7,6	458±23	227±11	629±31	327±16
As		68±3,4								38±3,1	19±2,9	32±2,6	38±3,1	24±2,9	
Rb	27±1,4	29±1,5	42±2,1	45±2,25	50±2,5	52±2,6	76±3,8	40±2	83±4,15	7,9±0,88	7,5±0,82	68±3,4	58±2,9	35±1,7	59±2,9
Sr	101±10									213±10	200±10		145±17	303±15	87±4,3
Zr	485±24	167±12	121±6	234±12	161±8	569±28,45	228±11,4	204±10,2	194±9,7	226±11	211±12	106±9,5	139±9,7	199±12	164±9,8
Sb	0,39±0,02	1,4±0,072	1,1±0,06	1,9±0,09	1,5±0,08	0,4±0,02	0,6±0,03	4±0,2	0,5±0,003	1,3±0,067	1,2±0,062	2,1±0,11	0,83±0,042	1,4±0,068	1,1±0,056
Cs	1,3±0,066	1,6±0,081	2,5±0,125	3,2±0,16	3,3±0,17	2,3±0,12	5,2±0,26	2,4±0,12	5,6±0,28	0,36±0,029	0,34±0,03	4,2±0,21	4,2±0,21	2,1±0,10	3,3±0,16
Ba	393±19	449±22	196±9,8	289±14,45	249±12,45	334±16,7	267±13	254±12,7	279±14	208±12	196±13	222±11	423±21	328±16	253±12
Hf	22±1,1	6,7±0,33	3,2±0,16	5,9±0,3	4,2±0,21	14±0,7	6,2±0,31	5,1±0,26	4,7±0,24	7,3±0,36	6,9±0,34	3,8±0,19	5,1±0,25	6,4±0,32	5,6±0,28
Ta	11±0,55	2,6±0,13	1,3±0,065	1,8±0,09	1,6±0,08	1,6±0,08	1,7±0,085	2±0,1	1,7±0,085	2,2±0,11	2,1±0,10	1,5±0,078	1,7±0,086	1,9±0,099	2,2±0,11
Ir											2,3±0,65	0,73±0,6	0,83±0,55	1,7±0,76	
Th	24±1,2	6,2±0,31	5,7±0,29	7,2±0,36	7,3±0,37	20±1,0	8,7±0,44	6,6±0,33	8,5±0,43	3,4±0,17	3,2±0,16	7,3±0,36	7,1±0,35	5,6±0,28	6,6±0,33
U	7,2±0,36	3,2±0,16	6,3±0,32	3,2±0,16	2,6±0,13	4,4±0,22	1,9±0,1	3,1±0,16	2,4±0,12	1,8±0,14	1,2±0,13	2,4±0,12	2,2±0,13	1,1±0,14	3,2±0,16
La	82±4,1	15±0,77								22±1,1	41±2,1	23±1,1	22±1,1	32±1,6	25±1,24
Ce	188±9,4	32±1,6	65±3,25	61±3,05	85±4,2	178±8,9	83±4,15	45±2,25	55±2,75	68±3,4	63±3,2	47±2,3	51±2,6	97±4,8	75±3,8
Nd	75±3,8	14±1,6	28±1,4	19±0,95	37±1,85	79±3,9	27±1,3	17±0,85	20±1,0	28±1,4	65±3,3	14±1,2	24±1,4	41±2,1	30±1,5
Sm	14±0,70	4,2±0,21								11±0,58	20±1,0	4,8±0,24	6,9±0,35	13±0,66	9,5±0,5
Eu	3,2±0,16	0,99±0,05	1,9±0,095	1,7±0,085	2,5±0,125	3,9±0,195	2,2±0,11	1,4±0,07	1,4±0,07	3,3±0,16	3,1±0,15	1,2±0,06	1,7±0,088	3,6±0,18	2,3±0,1
Gd	13±0,66	2,8±0,34								6,4±0,45	6,0±0,42	3,6±0,33	3,9±0,31	7,3±0,36	5,5±0,33
Tb	1,5±0,076	0,85±0,042	1±0,05	0,8±0,04	1,3±0,06	2,2±0,11	1,2±0,05	0,5±0,025	0,9±0,045	2,3±0,12	2,1±0,11	0,89±0,045	0,53±0,026	2,3±0,12	0,71±0,036
Dy	11±0,57	4,1±0,20								8,9±0,45	18±0,93	4,3±0,21	8,9±0,45	11±0,55	7,3±0,36
Yb	4,5±0,23	1,2±0,061	0,8±0,04	1,3±0,10	1,3±0,10	4,4±0,02	1,6±0,08	0,9±0,045	1,50±0,075	1,3±0,10	1,2±0,098	1,8±0,089	1,5±0,075	1,9±0,099	1,2±0,098
Lu	0,62±0,031	0,2±0,01								0,31±0,015	0,42±0,021	0,31±0,015	0,4±0,02	0,33±0,017	0,37±0,019

Table 4.
Trace element concentrations of bentonite layers from an outcrop 800 m NW of the Anthering section.

ANTHERING BENTONITES									
y-values ppm, except declared with %									
	y1	y3	y4	y6	y7	y10	y11	y12	y13
Sc	7,7±0,4	24±1,2	26±1,3	23±1,1	14±0,7	41±2,0	41±2,0	41±2,0	42±2,1
V	34±3,1	224±11	267±13	535±27	141±7,1	414±21	438±22	407±20	465±23
Cr	12±0,6	73±3,6	73±3,6	60±3,0	78±3,9	106±5,3	109±5,4	112±5,6	109±5,5
Mn	75±3,8	56±2,8	67±3,3	146±7,3	419±21	148±7,4	47±2,3	26±1,6	39±1,9
Fe %	3,1±0,2	5,2±0,3	4,7±0,2	5,8±0,3	2,4±0,1	4,4±0,2	3,9±0,2	3,6±0,2	4,0±0,2
Co	3,4±0,2	37±1,8	59±2,9	26±1,3	7,1±0,4	17±0,8	14±0,7	4,5±0,2	9,6±0,5
Ni	44±2,2	93±6,5	107±7,4	28±1,4	66±4,6	47±2,3	77±3,9	55±2,7	59±2,9
Zn	291±15	477±24	361±18	39±1,9	133±6,6	166±8,3	149±7,5	166±8,3	179±8,9
As	>8	14±2,1	35±2,4	16±0,8	>9	15±2,6	27±2,4	12±2,0	31±2,5
Rb	22±1,1	25±1,3	47±2,3	31±1,5	45±2,2	8,1±0,4	10±0,9	10±0,8	9,2±0,8
Sr	897±45	354±18	384±19	282±14	249±15	201±22	303±27	153±21	72±3,6
Zr	418±21	159±9,6	167±9,9	128±7,7	929±46	217±13	211±12	204±12	203±10
Sb	0,62±0,1	1,1±0,1	2,0±0,1	1,4±0,1	0,55±0,03	0,83±0,04	0,84±0,04	0,75±0,04	0,76±0,04
Cs	0,77±0,1	1,6±0,1	2,7±0,1	1,8±0,1	1,6±0,1	0,28±0,03	0,21±0,03	0,31±0,03	0,29±0,03
Ba	422±21	273±13	279±14	342±17	490±24	252±12	329±16	420±21	270±13
Hf	21±1,1	4,9±0,3	5,7±0,3	4,5±0,2	27±1,3	6,9±0,3	6,9±0,4	7,2±0,4	7,1±0,4
Ta	10±0,5	1,9±0,1	2,1±0,1	2,0±0,1	1,9±0,1	2,3±0,1	2,3±0,1	2,3±0,1	2,3±0,1
Th	23±1,1	4,8±0,3	6,2±0,3	3,1±0,2	29±1,5	3,4±0,2	3,5±0,2	3,8±0,2	3,5±0,2
U	6,1±0,3	1,7±0,1	1,5±0,1	1,5±0,2	7,2±0,5	1,5±0,1	1,9±0,1	2,3±0,2	2,1±0,2
La	46±2,3	28±1,4	28±1,4	10±0,5	90±4,5	24±1,2	22±1,1	29±1,4	27±1,3
Ce	122±6,1	77±3,8	85±4,2	22±1,1	206±10	75±3,7	65±3,3	77±3,9	78±3,9
Nd	42±2,1	38±1,9	41±2,1	10±0,5	91±9,1	37±1,8	39±1,9	43±2,2	46±2,3
Sm	9,5±0,5	11±0,6	11±0,6	2,6±0,1	22±1,1	13±0,7	12±0,6	15±0,8	15±0,8
Eu	2,2±0,1	2,9±0,2	2,9±0,1	0,73±0,04	3,6±0,2	3,6±0,2	3,4±0,2	4,1±0,2	3,9±0,2
Gd	15±0,8	8,3±0,4	5,8±0,4	1,7±0,1	19±1,0	6,8±0,4	6,8±0,5	8,4±0,5	7,3±0,5
Tb	1,1±0,1	1,1±0,1	1,7±0,1	0,52±0,03	2,7±0,1	0,99±0,05	2,3±0,1	1,3±0,1	2,7±0,1
Dy	8,3±0,4	6,9±0,4	7,7±0,4	1,7±0,2	17±0,9	9,5±0,5	8,8±0,4	11±0,5	11±0,5
Yb	5,2±0,3	1,5±0,1	1,4±0,1	0,35±0,09	7,7±0,4	1,3±0,1	1,4±0,1	1,9±0,1	1,5±0,1
Lu	0,88±0,1	0,30±0,05	0,36±0,02	0,38±0,02	0,92±0,05	0,41±0,02	0,39±0,02	0,33±0,02	0,43±0,02

tron Activation Analysis (NAA) in two analytical runs. For short time NAA, the samples were weighed (about 100 mg each) into polyethylene capsules, for the longer irradiation quartz glass ampoules (Suprasil) were applied. The irradiations were performed in the irradiation facilities of the TRIGA Mk II reactor of the Atominstitut der Österreichischen Universitäten in Vienna and at the ASTRA reactor of the Austrian Forschungszentrum Seibersdorf. The neutron fluxes were $2{,}5\times e10^{12}$ cm^{-2} s^{-1} and 7×10^{13} cm^{-2} s^{-1}, respectively gamma-spectrometric measurements were performed after convenient decay times with a HPGe detector and a PC-based gamma-spectroscopy system.

The Ti, Zr, Nb and Y analyses were performed on a sequential X-ray spectrometer Philips 2400 with a Rh-anode and a Philips Super Q, version 1.1 software as evaluation program. For preparation the ground sample was added to a polyvinyl alcohol solution (binding agent) and the well-mixed blend was pressed to pellets and dried at 70°C.

With SiO_2 values ranging from 56 % to 65 % (Table 5) the bulk sample major-element analyses of the bentonite layers refer to an andesitic to dacitic composition of the ash material. Due to the total conversion of the ashes to smectitic clay however the original chemical composition of the layers has strongly changed. Therefore only immobile elements can be used as indicators for the original material.

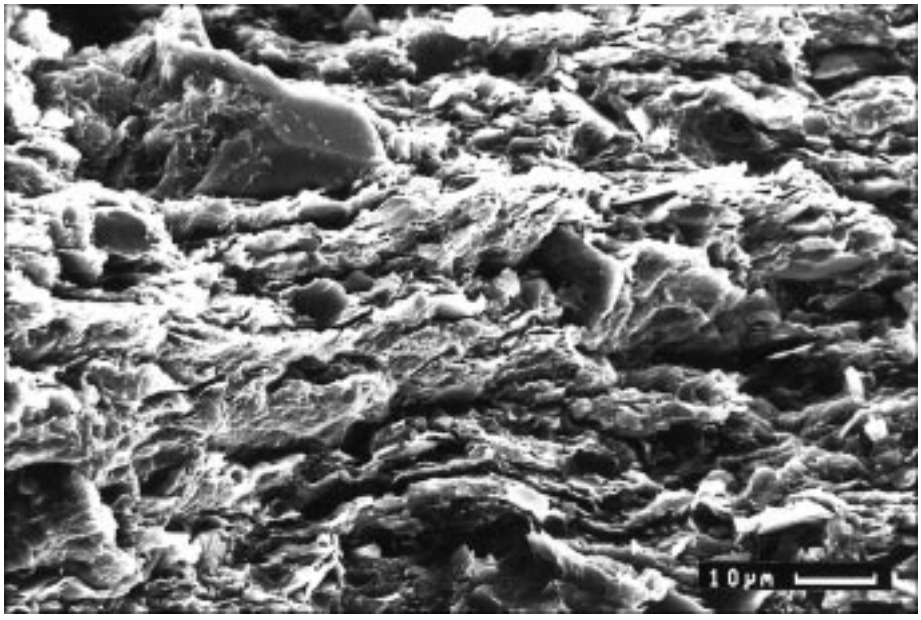

Text-Fig. 5.
SEM image of a bentonite from the Anthering section.

Table 5.
Major element analyses of bentonites normalized to 100 % without loss on ignition (LOI).

	x4	x11	x16
SiO_2	65	62.3	58.6
TiO_2	1.24	1.74	4.35
Al_2O_3	22	17.6	21.6
Fe_2O_3	4.83	9.7	7.15
MnO	0.01	0.05	0.01
MgO	2.64	2.27	2.37
CaO	2.41	2.63	1.31
Na_2O	0.83	0.26	1.17
K_2O	0.87	2.84	1.31
P_2O_5	0.17	0.23	0.25
LOI	14.12	10.52	11.34

The ashes of the Anthering formation have been divided into two groups, for which geochemical results are presented in Tables 3, 4, 5. Dominating are ashes with high Ti and V values and low Zr, Hf, Ta and Th concentrations. Contrary to that composition a few layers display low V contents and high concentrations of Zr, Hf Ta and Th, trace elements that are typically abundant in alkaline rocks. Usually the bentonites of the first group are very thin (less than 0,5 cm) whereas the ashes of the second group show thicknesses up to 3 cm.

In the Zr/TiO_2 – Nb/Y diagram, the first group of ashes plots in the alkali basalt field (Text-Fig. 6), the composition of the sporadic thicker layers, however, falls into the trachyte field. So it is obvious that the bentonites of the Anthering section display mainly basaltic compositions and only a few highly evolved alkaline ashes are present as well.

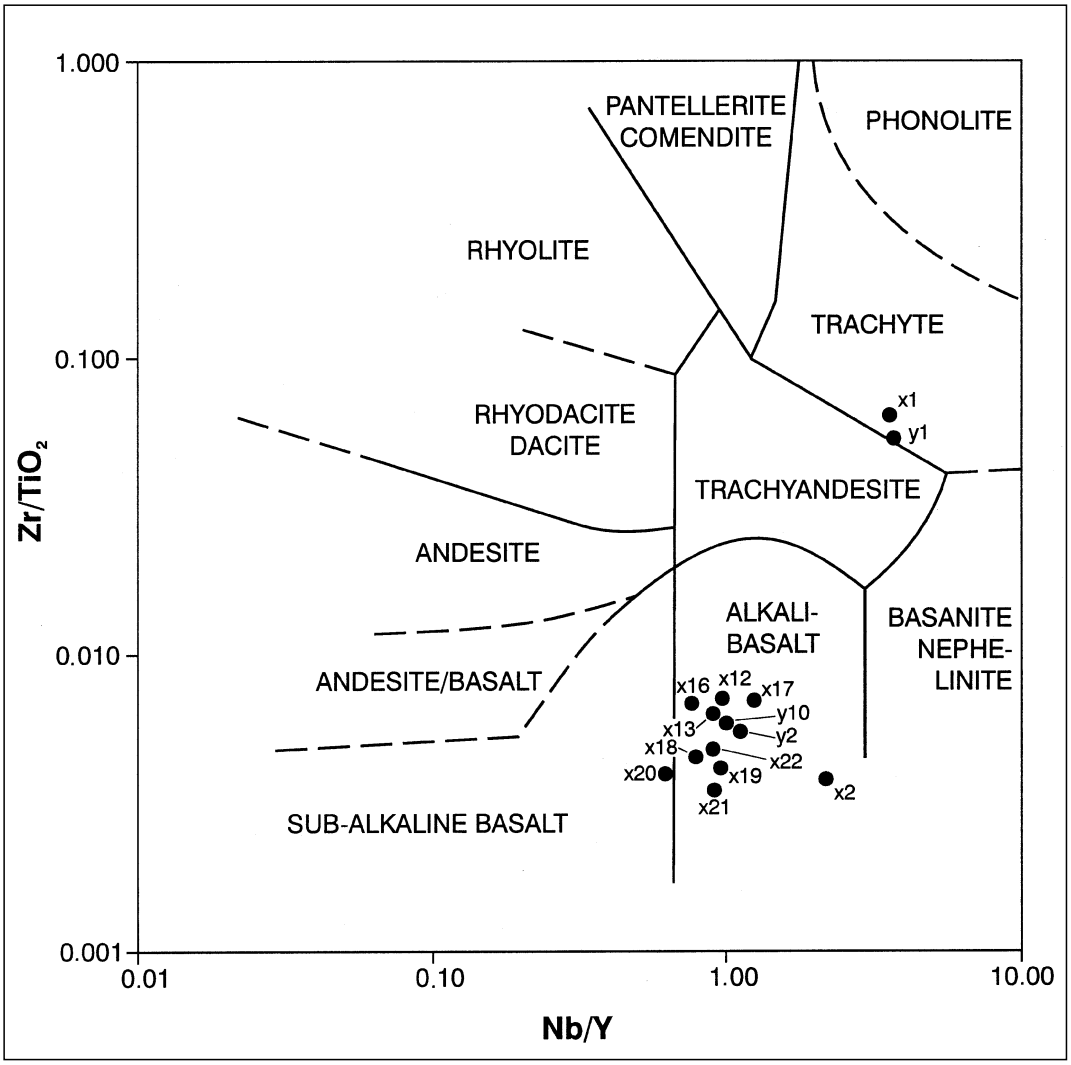

Text-Fig. 6.
Magma origin of different ash layers of the Anthering formation by means of immobile element distribution (see WINCHESTER & FLOYD, 1977).

3. Biostratigraphy of the Ash-Bearing Sequence

3.1. Calcareous Nannofossil Stratigraphy

Calcareous nannofossils were examined with a Zeiss photomicroscope. In the studied samples both diversity and abundance of calcareous nannoplankton are generally high, the majority of the samples are showing only moderate preservation however (Plate 1). All samples display contents of reworked species mainly from the Campanian and Maastrichtian but also Lower Cretaceous species were observed. A detailed inventory of the observed species will be published in a separate paper. Here we will refer only to the biostratigraphic important taxa which are used for determining the age of the ash series.

The beginning of the ash series lies in the uppermost part of outcrop H. In the samples of the marls adjoining the oldest bentonites (layers x1, x2 and x3) beside common *Discoaster multiradiatus* specimens *Tribrachiatus bramlettei* and *Discoaster diastypus* (see Plate 1) do already occur. Therefore it is obvious that the beginning of the increased explosive volcanic activity lies within NP 10. In the lower part of outcrop H (approximately 10 m below layer 1) specimens questionably assignable to *T. bramlettei* were observed. There seems to be an evolutionary transition between the

genus *Tribrachiatus* and *Rhomboaster* and therefore the first occurrence of *Tribrachiatus* is very difficult to recognize. As no specimens of *Tribrachiatus* were observed in outcrops I and J the NP 9/NP 10 boundary is drawn in the lower part of outcrop H. Around the NP 9/NP 10 boundary *Transversopontis pulcher* is a common species and in a few samples *Rhabdosphaera solus* is also common.

In this older part of the section (J, I, lower H) a large number of redeposited specimens was observed. This is probably an effect of low plankton productivity in the uppermost Paleocene because in that part of the section claystones are very common whereas mudturbidites are rather rare. Beside *Tribrachiatus* and *Rhomboaster* stratigraphically important species are *Fasciculithus involutus*, *F. schaubii*, *Toweius eminens*, *Campylosphaera eodela*, *Ellipsolithus distichus*, *E. macellus* and *Heliolithus kleinpelli*. Except of *F. schaubii* all named taxa were found also in the samples of outcrops G, F and E. Therefore we can assume that these taxa cross the NP 9/NP 10 boundary and have their last occurrence in the early NP 10. *Discoaster binodosus* has its first appearance in the samples of the outcrop G.

T. bramlettei is rare also in the younger sediments farther downstream and becomes more common in the upper part of outcrop E and especially in the lower part of outcrop D. Bentonites are still common in outcrop E but none of them were found in outcrops D, C, B and A. The first occurrence of *T. contortus* is within outcrop D 3 m to 4 m above the ash series. Together with *T. contortus* a smaller representative of the genus *Tribrachiatus* appears. This is described as *T. digitalis* by AUBRY et al. (1996). According to this author *T. digitalis* has a narrow stratigraphic range immediately before the first appearance of *T. contortus*. In our samples however, *T. digitalis* co-occurs with *T. contortus*. This may be an effect of redepostion but it is also often very difficult to distinguish between both morphotypes. Therefore we prefer the name *T. contortus* for both variations which we call A (= *digitalis*) and B (= *contortus*). It is obvious that the first appearance of *T. contortus* postdates the ash series which is therefore restricted to the lowermost part of NP 10.

Sediments from NP 10 are exposed also in outcrops C and B where *T. contortus* co-occurs with *T. orthostylus*. It is remarkable that *Sphenolithus editus* has its first appearance in that part of the section. The total thickness of NP 10 comes up to 60 m in the Kohlbach section. Within outcrop B lies the boundary to NP 11 where *T. contortus* has vanished and only *T. orthostylus* was observed. As in all other outcrops of the Anthering section *Discoaster multiradiatus* and *Chiasmolithus bidens* are common species.

3.2. Palynology

Two samples from the black shales of outcrop E have been examined palynologically. For the first time dinoflagellates and sporomorphs from the Paleogene of the Rhenodanubian flysch are described here. Standard processing methods with HCl, hydrofluoric acid, azetolysis and heavy liquid separation (bromoform-alcohol separation without sieving) were used.

The organic residue in the palynological preparations includes terrestrially derived particles (fragments of amorphous darkbrown particles, yellow to lightbrown plant cuticles, wood tissue, tracheidal matter), which are dominating over the palynomorphs. The palynoflora contains an assemblage with pollen and spores (31 %) and abundant dinoflagellates (69 %). The dominance of the organic walled microplankton is typical for a marine depositional environment.

Due to the anoxic conditions at the basin floor the dinoflagellates and sporomorphs are often filled with pyrite (Plate 2,3). Therefore the preservation of the palynomorphs is poor. Owing to their fragile exines they are usually damaged and corroded and therefore especially the pollengrains are often undeterminable. Additional damage may be caused by mechanical abrasion during the long distance transportation of the grains. In general the thickwalled fern spores are better preserved than the pollengrains.

The sporomorphs are dominated by angiosperms and pteridophytes whereas gymnospermes are less important. Due to their bad preservation the pollengrains very often could not be determined or only the family or genus could be identified using the scanning electron microscope.

The pollen assemblage of the samples from Anthering is dominated by many triporate juglandaceous pollentypes belonging to *Carya, Platycarya, Engelhardia* (*Momipites* sp.) and Myricaceae (*Triatriopollenites* sp.). Most of the representatives of this group have their first appearance in the late Paleocene. Angiosperms are also represented by specimens of the families Fagaceae, Betulaceae (*Alnus* sp.), Olaeceae, Tiliaceae, Verbenaceae, Icacinaceae (*Compositoipollenites* sp.), Anacardiaceae (*Rhus* sp.), Platanaceae, Aquifoliaceae (*Ilex* sp.) and Sapotaceae. Representatives of the *Normapolles* group, which had its highest diversity in the early Paleocene, are rare (*Pompeckjoidaepollenites subhercynicus, Plicapollis pseudoexcelsus*).

The pollen assemblage contains as well elements of the paleotropical vegetation like Icacinaceae (according to KRUTZSCH, 1967) as also elements of the arktotertiary vegetation like *Alnus*, Fagaceae and *Abies*.

Spores of gymnosperms include the families Pinaceae (*Pinus* sp., *Abies* sp.) and Taxodiaceae (*Taxodium* sp.). Pteridophytes are represented by the families Gleicheniaceae (*Concavisporites* sp.) and Schizeaceae (*Lygodium* sp., *Cicatricosisporites dorogensis, Varirugosporites* sp.).

The dinoflagellates include spiniferate, cavate, chorate and proximate cysts. There are a lot of spiniferate dinoflagellates in high frequency and diversity with simple and hooked spines. The most characteristic dinoflagellate taxa are the Wetzeliella forms belonging to the genus Apectodinium. Different species could be recognized in the samples in Anthering which belong to the *Apectodinium homomorphum* group in the sense of HARLAND. The intergradation from subspheroidal cyst bodies without horn to more pentagonal bodies with horns could be observed. Beside *Apectodinium homomorphum Apectodinium quinquelatum* could be determined. According to HEILMANN-CLAUSEN (1994) the base of *Apectodinium hyperacanthum* Zone is defined by the first occurrence of *Apectodinium homomorphum*. This biozone correlates with nannoplankton zone NP 9. An acme of *Apectodinium* was observed around the Paleocene/Eocene boundary (HEILMANN-CLAUSEN, 1985).

Another dinoflagellate guide type is assigned to the species *Deflandrea oebisfeldenis*. HEILMANN-CLAUSEN (1985) pointed out that according to the original diagnosis the typical form of this species has reduced antapical horns. The periphragm could have spinules (Plate 1, Text-Fig. 2, 3) or be smooth. The specimens with well developed antapical horns might intercalate to the closely related *Ceratiopsis speciosa*. *Deflandrea oebisfeldensis* is known from the late Paleocene–early Eocene (NP 7–12) in NW Europe (HEIL-

MANN-CLAUSEN, 1985, WAAGSTEIN & HEILMANN-CLAUSEN, 1995).

These first palynological results from the Anthering section make us optimistic that a detailed biostratigraphic correlation between the boreal sections of the North Sea region (which are barren of calcareous plankton) and the Tethyan sections will be possible.

4. Discussion

A significant reduction of clastic input defines the lower boundary of the Anthering formation in the Late Paleocene. This change of sedimentary facies could be interpreted as a consequence of a transgression at the end of the Paleocene. During this sea level high stand siliciclastic sediments might have beeen stored on coastal plain, shoreline and inner shelf and were not transported to the shelfedge and from there to the adjacent basins. This interpretation is supported also by the high carbonate contents of the Anthering formation since the production of carbonate is highest during transgressions when the platform tops are flooded.Therefore more of this carbonate-rich mud is exported from there to the adjacent deep water areas (e.g. EBERLI, 1991, 349).

There are different opinions about the extent of sea level changes around the P/E boundary. The eustatic curves of HAQ et al. (1988) show three short term third order cycles at that time. The results from Caravaca in Spain (MOLINA et al., 1994) suggest a very high sea level rise already within the NP 9-zone at the time of the $\delta^{13}C$ negative excursion and the benthic foraminiferal extinction event. Results from Gebel Duwi in Egypt (SPEIJER et al., 1996) suggest only minor (10 m-20 m) sea level changes but even these will be sufficient for a significant change in sedimentary facies pattern. Therefore we expect that the particular facies of the Anthering formation is caused by oceanographic changes rather than by regional tectonic events.

The overall high contents of smectite in the pelitic rocks of the Anthering formation and the bentonite layers suggest that this transgression was associated with a strongly increased volcanic activity. It is not common that basaltic volcanism lead to widespread ash layers. Therefore MORTON & KEENE (1981) assume that the reason for the main phase of explosive volcanism in the North Sea region was water-magma interaction due to the subsidence of an active ridge below sea-level. It is noteworthy that this interval also marks a period of significant decrease in sedimentary output from the Scottish Highland and the Orkney-Shetland source areas (KNOX & MORTON, 1983). Both observations are consistent with the idea of a transgression at that time.

In the North Sea region the main volcanic phase took place around the Paleocene–Eocene transition. PEDERSEN & JÖRGENSEN (1981) distinguished between four successive volcanic stages. The ashes of the first three stages display mainly basaltic compositions. However, some highly evolved alkaline ashes are present as well. The fourth stage is characterized by a very high frequency in the eruptions (phase 2b of KNOX & MORTON, 1983), manifested in a monotonous sequence of 120 closely spaced tholeiitic basaltic layers (SCHMITZ & ASARO, 1996). The age and the geochemical characteristics of the first three volcanic stages in Northern Europe show a good correlation to the alpine bentonites. However, indications of the tholeiitic ashes of the fourth stage were not found at Anthering. This discrepancy is still an unsolved problem for the correlation of the bentonites from both areas.

Another problem rises from the results of a recent study on alpine bentonites: EGGER et al. (1996) describe bentonite layers within a marly shelf facies in the Northern Calcareous Alps about 15 km south of Anthering. The yellowish grey silty marls contain abundant calcareous nannoplankton. *Tribrachiatus bramlettei*, *Discoaster multiradiatus*, *Campylosphaera eodela*, *Rhomboaster cuspis* and *Fasciculithus involutus* are the stratigraphic important species which prove the lower part of biozone NP 9. *Rhomboaster* and *Pontosphaera* are usually found in shallow shelf areas and they are common in the Anthering section. As they are very rare in the section in the Northern Calcareous Alps a deeper environment as for the source area of the Anthering turbidites could be expected there. The geochemical correspondence of the samples from both sections suggests a common source of magma. In the Paleogene the Northern Calcareous Alps were located much farther in the south as the Rhenodanubian flysch. As the 12 bentonite layers from this outcrop are usually thicker (1–2 cm) than those of Anthering a source area in more southern latitude is expected.

A comparable conclusion was made by WINKLER (1983) and WINKLER et al. (1985) who gave the first description of Paleogene bentonites in the alpine region. These bentonites were found in the Wägital flysch in Switzerland which is regarded to be a western continuation of the Rhenodanubian flysch. There bentonites were deposited from the upper Maastrichtian to the early Eocene (NP 10–11). The latter have the same basaltic compositions as our bentonites at Anthering. Therefore a correlation between these two occurrences is highly probable. WINKLER et al. (1985) assume an origin of these ashes from the Veneto in Italy. There the volcanic activity started in the upper Paleocene and ended in the lower Miocene. However, in the Paleocene and Eocene mainly basaltic effusiva were produced whereas higher amounts of pyroclastics do not appear before the upper Eocene (BÜNTE, 1996). Therefore it is not probable that the source area for the bentonites in the alpine flysch deposits was located in that area.

Finally we can recapitulate that there are close similarities between the bentonite of the alpine region and the North Sea Basin but there are also a few unsolved problems with the correlation which have to be studied by further investigations.

Acknowledgments

We wish to thank W. SCHNABEL and H. STRADNER for helpful discussions and comments on the text. R. BARRIE (Levin, New Zealand) read part of the English text. This research was supported by FFWF grant P-8310–Geo.

References

AUBRY, M.-P. (in press): Towards an Upper Paleocene – Lower Eocene high resolution stratigraphy based on calcareous nannofossil stratigraphy. – Israel J. Earth Sci.

AUBRY, M.-P., BERGGREN, W.A., STOTT, L. & SINHA, A. (1996): The upper Paleocene – lower Eocene stratigraphic record and the Paleocene-Eocene boundary carbon isotope excursion: implications for geochronology. – In: KNOX, R.W.O'B., CORFIELD, R.M. & DUNAY, R.E. (eds.): Correlation of the Early Paleogene in Northwest Europe. – Spec. Publ. Geol. Soc., **101**, 353–380, London.

BERGGREN, W.A. & AUBRY, M.-P. (1996): A late Paleocene–early Eocene NW European and North Sea magnetochronological correlation network. – In: KNOX, R.W.O'B., CORFIELD, R.M. & DUNAY, R.E.: Correlation of the Early Paleogene in Northwest Europe, Spec. Publ. Geol. Soc., **101**, 309–352, London.

BERGGREN, W.A. & MILLER, K.G. (1988): Paleogene planktonic foraminiferal biostratigraphy and magnetobiochronology. – Micropaleont., **34**, 362–380, Amsterdam.

BERNER, R.A. (1970): Sedimentary pyrite formation. – Am. Jour. Sci., **268**, 1–23, Washington.

BUKRY, D. (1973): Low-latitude coccolith biostratigraphic zonation. – Initial reports Deep Sea drill. proj., **15**, 685–703, Washington.

BÜNTE (1996): Geochemische und petrographische Untersuchungen an den basaltischen Gesteinen der tertiären Vulkanit-Provinz des Veneto (Nord-Italien). – Münster Forsch. Geol. Paläont., **79**, 136p., Münster.

DILL (1986): Metallogenesis of early Palaeozoic graptolite shales from the Graefenthal Horst (northern Bavaria - Federal Republic of Germany). – Economic Geol., **81**, 889-903, Lodnon.

EBERLI, G.P. (1991): Calcareous turbidites and their relationship to sea-level fluctuations and tectonism. – In: EINSELE, G., RICKEN, W. & SEILACHER, A. (1991): Cycles and events in stratigraphy, 340–359, Berlin (Springer).

EGGER, H. (1995): Die Lithostratigraphie der Altlengbach-Formation und der Anthering-Formation im Rhenodanubischen Flysch (Ostalpen, Penninikum). – N. Jb. Geol. Paläont. Abh., **196**, 69–91, 1 Tab., Stuttgart.

EGGER, H. (1996): Late Paleocene to early Eocene flysch deposits of the Austrian Alps. – In: MOLINA, E., SCHMITZ, B. & LUTERBACHER, H. (eds.): Early Paleogene stage boundaries, Abstracts, **15**, Zaragoza.

EGGER, H., BICHLER, M., HOMAYOUN, M., KIRCHNER, E.CH. & SURENIAN, R. (1996): Spätpaleozäne Bentonite aus der Gosau-Gruppe des Untersberg-Vorlandes (Nördliche Kalkalpen, Salzburg). – Jb. Geol. B.-A., **139**, 13–20, Wien.

HAQ, B.U., HARDENBOL, J. & VAIL, P.R. (1988): Mesozoic and Kenozoic chronostratigraphy and cycles of sea-level change. – Spec. Publ. Soc. Econ. Paleont. Mineral., **42**, 71–108, Tulsa.

HEILMANN-CLAUSEN, C. (1985): Dinoflagellate stratigraphy of the uppermost Danian to Ypresian in the Viborg 1 borehole, central Jylland,Denmark. – Danm. Geol. Unders, serie A, **7**, 1–69, Kopenhagen.

HEILMANN-CLAUSEN, C. (1994): Review of Paleocene dinoflagellates from the North Sea Region. – Meeting proceedings "Stratigraphy of the Paleocene", GFF 116, 51–53.

KNOX, R.W.O'B. & MORTON, A.C. (1983): Stratigraphical distribution of early paleogene pyroclastic deposits in the North sea basin. – Proc. Yorkshire Geol. Soc., **44**, 355–363, Yorkshire.

KRUTZSCH, W. (1967): Der Florenwechsel im Alttertiär Mitteleuropas auf Grund von sporenpaläontologischen Untersuchungen. – Abh. zentr. geol. Inst., **10**, 17–37, Berlin.

MARTINI, E. (1971): Standard Tertiary and Quarternary calcareous nannoplankton zonation. – In: FARINACCHI (ed.): Proceedings II Planktonic Conference, Roma 1970, **2**, 739–785.

MOLINA, E., CANUDO, J.I., MARTINEZ-RUIZ, F. & NIEVES, O. (1994): Integrated stratigraphy across the Paleocene/Eocene boundary at Caravaca, southern Spain. – Eclogae geol. Helv., **87**/1, 47–61, Basel.

MOORE, D.M. & REYNOLDS, R.C. (1989): X-ray diffraction and the identification and analysis of clay minerals. – 332 p., Oxford Univ. Press.

MORTON, A.C. & KEENE, J.B. (1981): Paleogene pyroclastic volcanism in the southwest Rockall plateau. – Initial Rep. DSDP, **81**, 633– 641, Washington.

MUZYLOV, N. (1994): Late Paleogene anoxic events – evidence from nannofossils studies. – J. Nannoplankton Research, **16**/1, 17, London.

OKADA, H. & BUKRY, D. (1980): Supplementary modification and introduction of code numbers to the low-latitude coccolith biostratigraphic zonation (BUKRY, 1973, 1975). – Marine Micropaleont., **5**, 321–325, Amsterdam.

PEDERSEN & JÖRGENSEN (1981): A textural study of basaltic tephras from lower Tertiary diatomites in northern Denmark. – In: SELF, S. & SPARKS, R.S., J. (Eds.): Tephra studies, 213–218, Dordrecht.

RAISWELL, R., BUCKLEY, F., BERNER, R.A. & ANDERSON, T.F. (1988): Degree of pyritization of iron as a palaeoenvironmental indicator of bottom-water oxygenation. – J. sediment. Petrol., **58**/5, 812–819, Tulsa.

SCHMITZ, B. & ASARO, F. (1996): Iridium geochemistry of volcanic ash layers from the early Eocene rifting of the northeastern North Atlantic and some other Phanerozoic events. – Bull. Geol. Soc. Amer., **108**, 489–504.

SPEIJER, R.P., VAN DER ZWAAN, G.J. & SCHMITZ, B. (1996): The impact of Paleocene/Eocene boundary events on middle neritic benthic foraminiferal assemblages from Egypt. – Marine Micropaleont., **28**, 99–132, Amsterdam.

SWISHER & KNOX (1991): The age of the Paleocene/Eocene boundary: $^{40}Ar/^{39}Ar$ dating of the lower part of NP 10, North Sea Basin and Denmark. – In: IGCP 308 (Paleocene/Eocene Boundary Events), Internation. Annual Meeting and Field Conference (Abstracts) Brussels.

THOREZ, J. (1976): Practical identification of clay minerals. A handbook for teachers and students in clay mineralogy. – 90 S., Lelotte, Dison.

WAAGSTEIN, R. & HEILMANN-CLAUSEN, C. (1995): Petrography and biostratigraphy of Paleogene volcaniclastic sediments dredged from the Faeroes shelf. – In: SCRUTTON, R.A., STOKER, M.S., SHIMMIELD, G.B. & TUDHOPE, A.W. (eds.): The tectonics, sedimentation and Palaeoceanography of the North Atlantic region, Spec. Publ. Geol. Soc., **90**, 179–197, London.

WIGNALL, P.B. (1994): Black Shales. – Oxford monographs geol. geophysics, **30**, 127p., Oxford (Clarendon press).

WINCHESTER, J.A. & FLOYD, P.A. (1977): Geochemical discrimination of different magma series and their differentiation products using immobile elements. – Chem. Geol., **20**, 325–343, Amsterdam.

WINKLER, W. (1993): Control factors on turbidite sedimentation in a deep-sea trench setting. The example of the Schlieren Flysch (Upper Maastrichtian–Lower Eocene, Central Switzerland). – Geodinamica Acta, 1993, **6**, 81–102, Paris.

WINKLER, W. (1983): Stratigraphie, Sedimentologie und Sedimentpetrographie des Schlieren-Flysches (Zentralschweiz). – Beitr. Geol. Karte Schweiz, N.F., **158**. Lieferung, 105 p., Bern.

WINKLER, W., GALETTI, G. & MAGGETTI, M. (1985): Bentonite im Gurnigel-, Schlieren- und Wägitalflysch: Mineralogie, Chemismus, Herkunft. – Eclogae Geol. Helv., **78**, 545–564, Basel.

Manuskript bei der Schriftleitung eingelangt am 6. Februar 1997

Plate 1

Calcareous nannoplankton from the Anthering section.

Fig. 1: *Tribrachiatus orthostylus* (Type B).
Fig. 2: *Tribrachiatus orthostylus* (Type A).
Fig. 3: *Tribrachiatus orthostylus* (Type A).
Fig. 4: *Tribrachiatus „digitalis“* (overgrown).
Fig. 5: *Tribrachiatus „digitalis“*.
Fig. 6: *Tribrachiatus contortus*.
Fig. 7: *Tribrachiatus bramlettei*.
Fig. 8: *Tribrachiatus contortus*.
Fig. 9: *Rhomboaster cuspis*.
Fig. 10: *Discoaster salisburgensis*.
Fig. 11: *Discoaster multiradiatus*.
Fig. 12: *Discoaster diastypus*.
Fig. 13: *Discoaster binodosus*.
Fig. 14: *Discoaster mediosus*.
Fig. 15: *Discoaster lenticulanus*.
Fig. 16: *Ellipsolithus distichus*.
Fig. 17: *Ellipsolithus macellus*.
Fig. 18: *Fasciculithus schaubii*.
Fig. 19: *Fasciculithus involutus*.
Fig. 20: *Campylosphaera eodela*.
Fig. 21: *Toweius eminens*.
Fig. 22: *Heliolithus kleinpelli*.
Fig. 23: *Chiasmolithus bidens*.
Fig. 24: *Sphenolithus editus*.
Fig. 25: *Micrantholithus obtusus* (redeposited).
Fig. 26: *Eprolithus* sp. (redeposited).
Fig. 27: *Zygodiscus adamas*.
Fig. 28: *Transversopontis pulcher*.
Fig. 29: *Neochiastozygus junctus*.

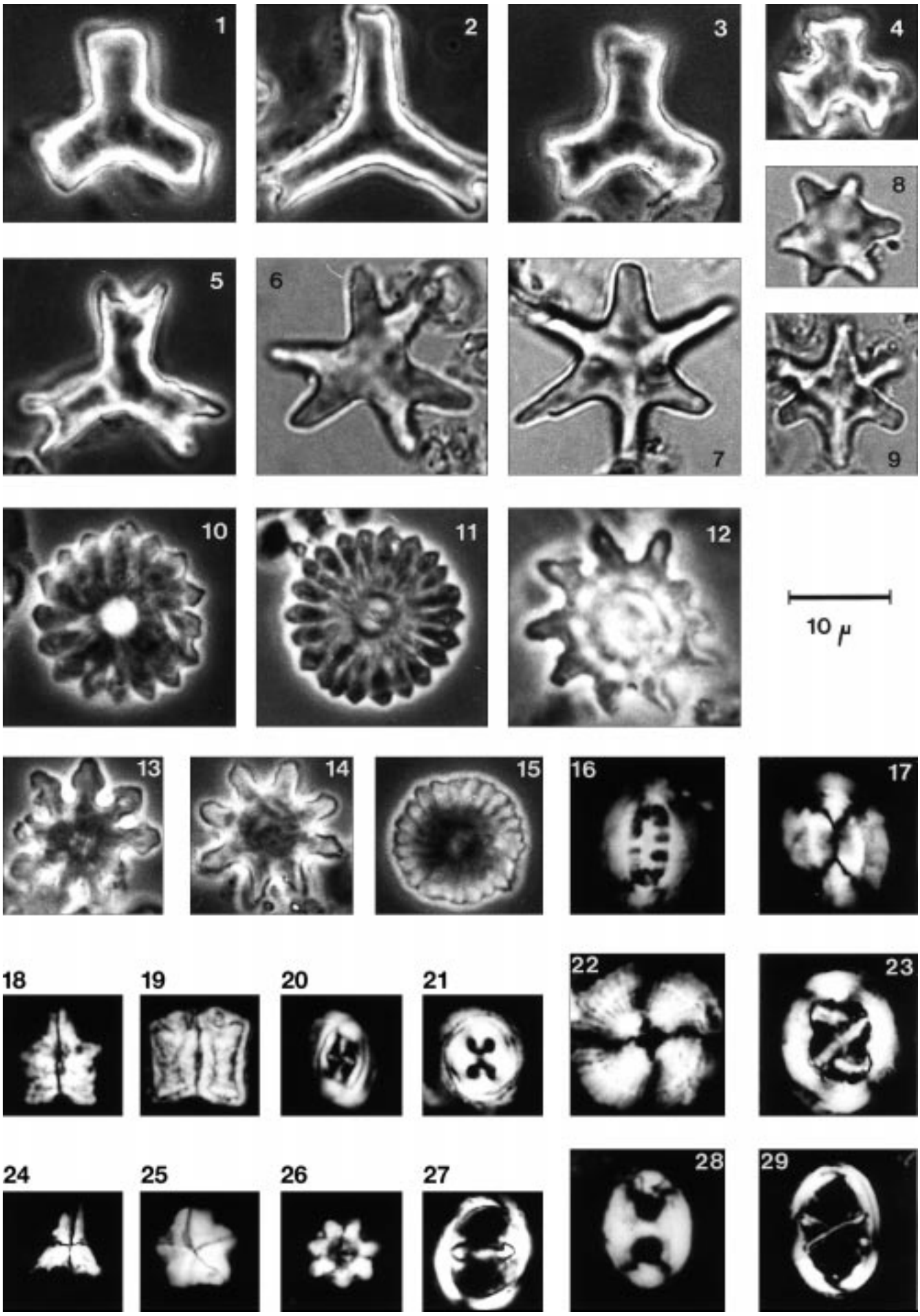
1
2
3
4
8
5
6
7
9
10
11
12
10 μ
13
14
15
16
17
18
19
20
21
22
23
24
25
26
27
28
29

Plate 2

Sporomorphs from the Anthering section.

Figs. 1– 3: Pteridophytic spore (Schizaeaceae-type).
Figs. 4– 6: Anacardiaceae (*Rhus* sp.).
Figs. 7– 9: cf. *Pompeckjoidaepollenites* sp.
Figs. 10–12: *„Postnormapolles“*.

Magnification according to the scale.

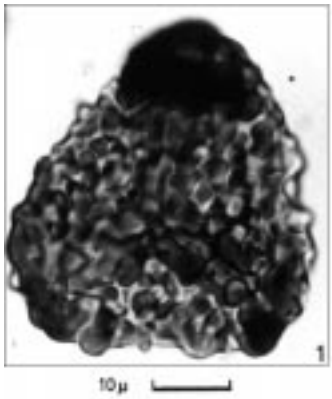
1
10μ

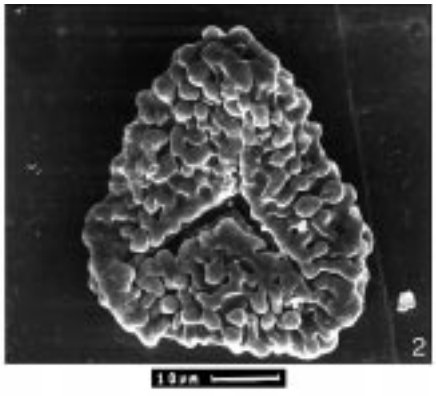
2
10μm

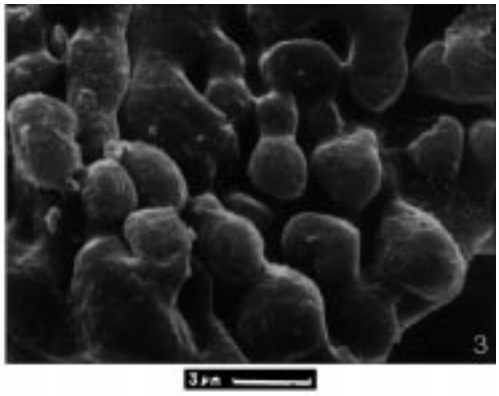
3
3μm


4
10μ

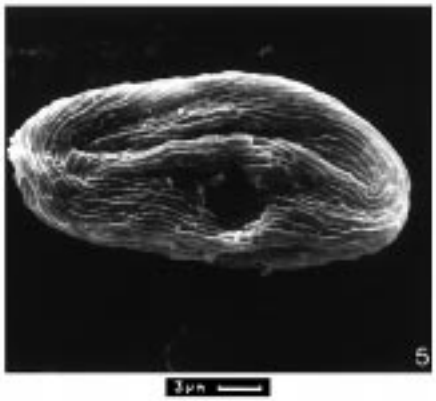
5
3μm

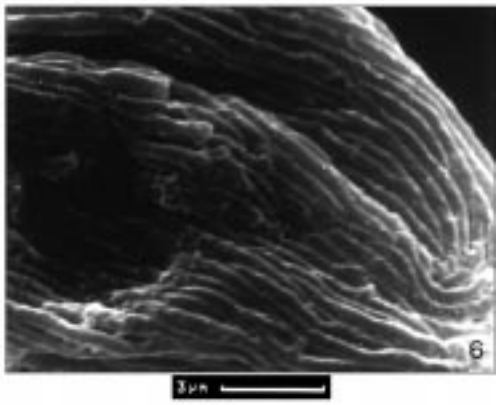
6
3μm

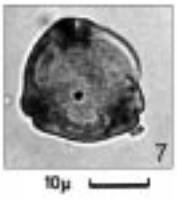
7
10μ

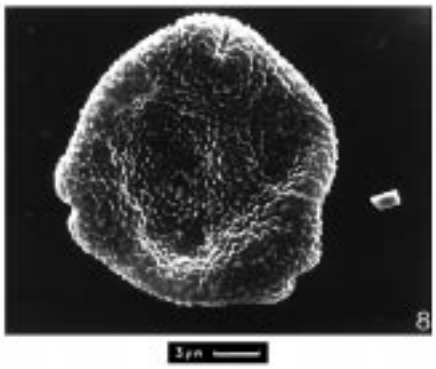
8
3μm

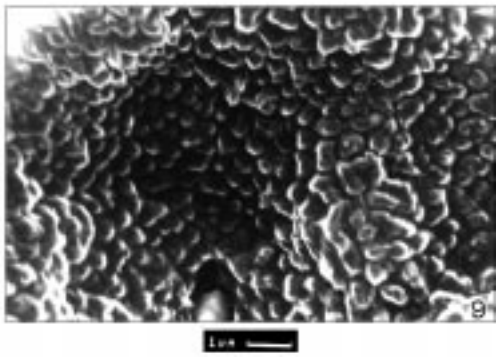
9
1μm

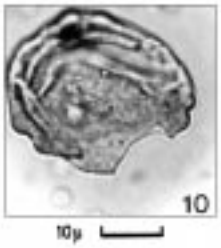
10
10μ

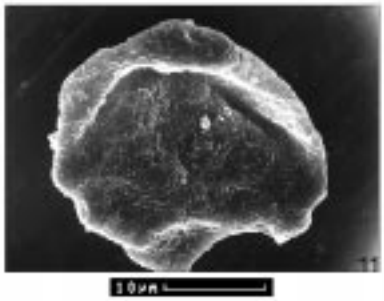
11
10μm

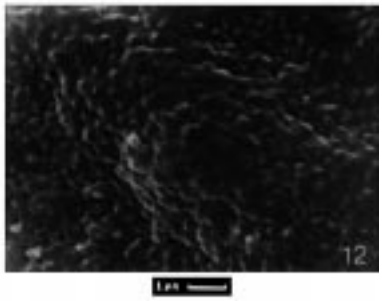
12
1μm


13
10μ

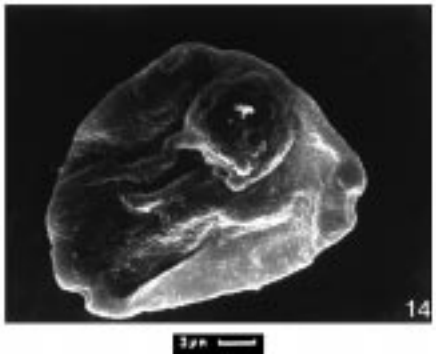
14
3μm

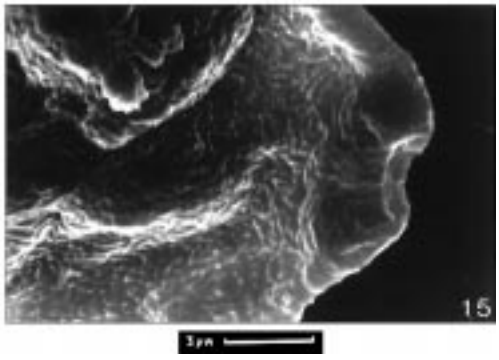
15
3μm

Plate 3

Dinoflagellates from the Anthering section.

Figs. 1–4: *Deflandrea oebisfeldensis* ALBERT.
Figs. 3,4: Same magnification.
Figs. 5–7: *Apectodinium* sp.
Figs. 8–9: Proximate dinoflagellate cyst.
Figs. 10,11–13,14–16: Spiniferites group, dinoflagellate cysts.

Magnification according to the scale.

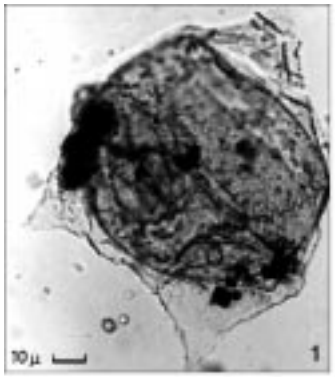
10µ
1

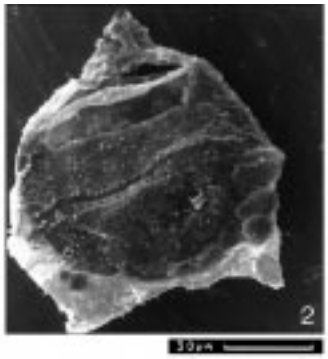
2

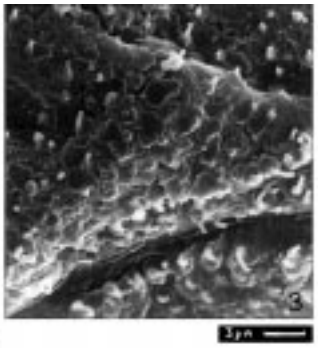
3

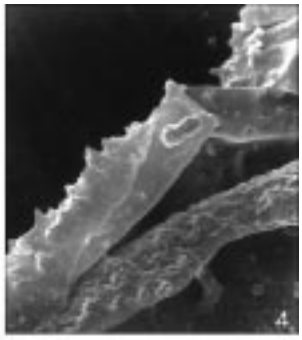
4

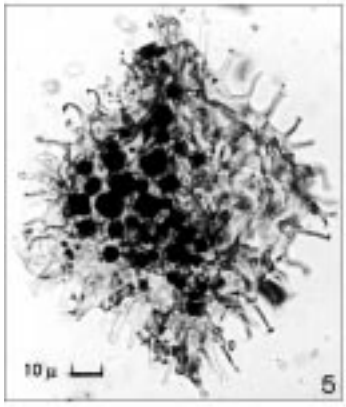
10µ
5

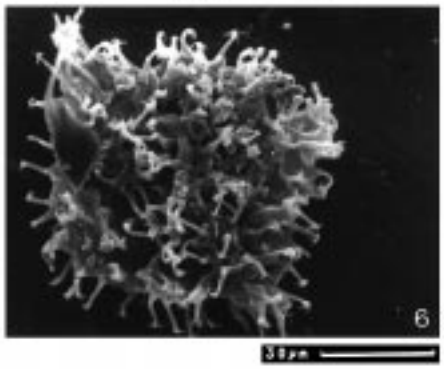
6

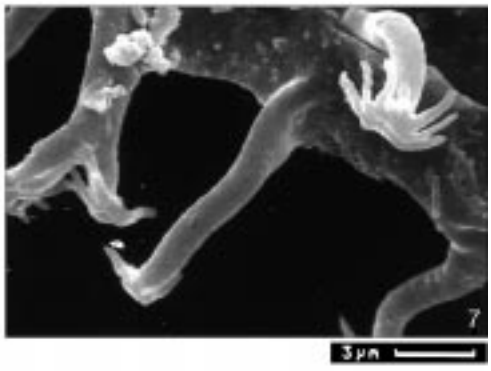
7
3µm

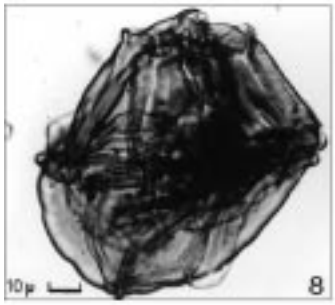
10µ
8


9

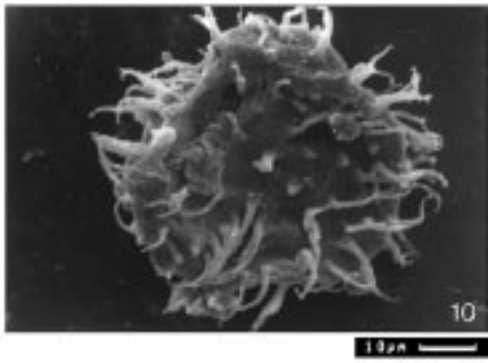
10

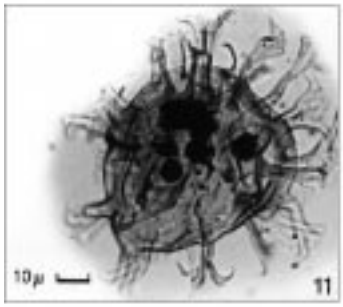
10µ
11

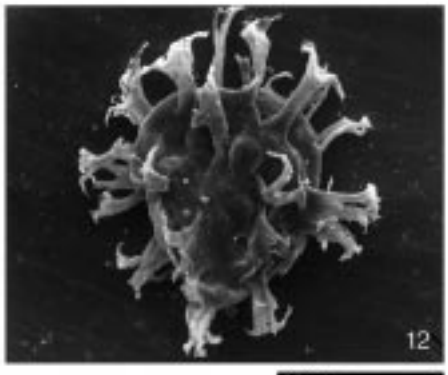
12

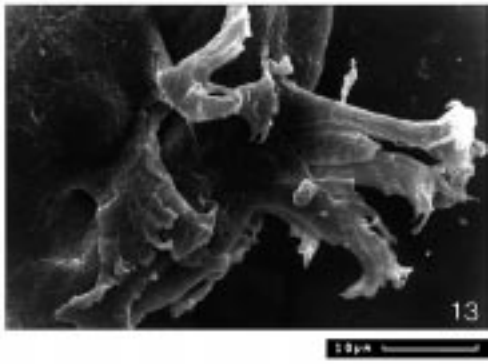
13

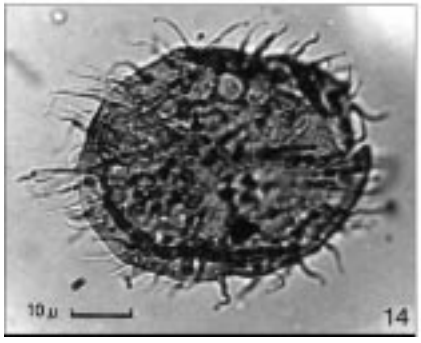
10µ
14

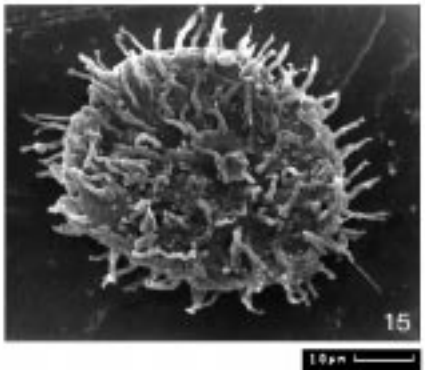
15